Received: 11 September 2019 | Revised: 4 October 2019 | Accepted: 16 October 2019

DOI: 10.1002/est2.103

RESEARCH ARTICLE

ENERGY STORAGE WILEY

Thermodynamic analysis of a hybrid energy system using geothermal and solar energy sources with thermal storage in a residential building

Shaimaa Seyam | **Ibrahim Dincer** | **Martin Agelin-Chaab**

Department of Automotive, Mechanical and Manufacturing Engineering, Faculty of Engineering and Applied Science, Ontario Tech University, Oshawa, Ontario, Canada

Correspondence
Shaimaa Seyam, Department of Automotive, Mechanical and Manufacturing Engineering, Faculty of Engineering and Applied Science, Ontario Tech University, Oshawa, Ontario, Canada.
Email: shaimaa.seyam@ontariotechu.net

Funding information
Natural Sciences and Engineering Research Council of Canada (NSERC)

Abstract

Residential buildings in Canada require remarkable heating loads in the winter. Many homeowners potentially consider more cost effective and environmentally-benign solutions, including solar energy systems, in order to replace fossil fuels. However, this might not be efficient because many cities are exposed to minimum solar radiation resulting in large surface area of solar panels. Therefore, a hybrid energy system is designed to combine five photovoltaic thermal solar panels, a 300-m geothermal loop, and 9463.53-kg water of phase change material thermal battery storage for a residential building of 325 m^2 total floor space in the city of Oshawa, Canada. The building has maximum heating and cooling loads of 13.8 and 8.7 kW, respectively. A thermodynamic analysis is applied to the system in January and the whole year. It was found that the solar panels can supply thermal energy and electrical power of 8 and 50 W, respectively, in January, while the geothermal and thermal storage energy can provide 16.8 and 9 kW over the year, respectively. The hybrid system requires an additional heating load of 1.85 kW from the furnace. The overall energetic and exergetic coefficient of performance of the system are estimated to be 54.58% and 3.34% in the winter and 42.6% and 4.47% in the summer, respectively.

KEYWORDS

efficiency, energy storage, exergy, geothermal energy, heat pump, photovoltaics, solar energy

1 | INTRODUCTION

Living in a cold climate requires space heating and water heating to achieve thermal comfort in residential buildings. Space heating accounts for a remarkable percentage of 62% of the total energy use, while water heating accounts for 19% of total energy use in Canadian homes.[1] Conventional fossil fuel-based energy sources, such as natural gas, are used for space heating because of its low cost. However, fossil fuels emit harmful gases to the atmosphere causing global warming, air pollution, and acid rain, which have negative effects on human health.[2] In order to reduce building energy consumption and the negative impact on the environment, researchers and authorities are forced to find alternative solutions using environment-friendly and sustainable energy sources to cover a substantial part of their energy needs.

Solar energy is recognized as one of the most viable renewable-based energy sources because it is clean, inexhaustible, affordable, and free from regional restriction and high quality. This energy can be a source of electricity by using photovoltaic solar panels,[3] a source of heat as

in solar collectors,[4,5] or both as in photovoltaic thermal (PVT) solar collectors.[6-8] Solar panels can be combined with heat pump systems, which is an effective way to exploit the solar energy for air-conditioning residential spaces for both heating and cooling seasons.[9-11] However, solar energy is significantly changed according to temporal, spatial, and climatic conditions. Therefore, a supplement heat source is required to ensure the continuity and reliability of operating such systems.

The most challenging part of utilizing renewable energy systems is continuity and reliability for long operation period with the required energy load. Intensive research has been conducted in order to provide suitable and sustainable solutions such as geothermal wells, which can be combined with heat pump systems referred to as a ground source heat pump (GSHP).[11,12] GSHP systems are a promising technology that can take advantage of the ground both as a heat source and as a heat sink for energy storage. Since heat pump systems are affected on the air temperature, it is recommended to obtain constant surrounding conditions in order to achieve the more stable performance of heat pump systems with less environmental impact.[12] GSHP systems can fulfill this condition since the fluctuation in the ground temperature can be neglected although the ground temperature usually increases with a depth reaching a gradient of about 0.03°C/m. That means the ground temperature can reach to 70°C to 90°C even at shallow depths (100-200 m).[13]

Many researchers have investigated integrated renewable energy systems by combining solar energy and GSHP. For examples, Watzlaf and Ackman[14] have exploited mine water in geothermal heat pump systems for both heating and cooling buildings in Pennsylvania. The proposed systems have reduced annual costs for heating by 67% and cooling by 50% compared to the conventional method. In addition, Li and Sun[15] designed a ground-coupled heat system assisted by solar PVT system in a residential building in Beijing for space heating and domestic hot water. They have found that the integrated system has achieved a significant improvement in performance and energy-saving when domestic hot water dominates the heating load of the building. Liang et al.[16] proposed a solar assisted air heat pump system in order to improve the heating system performance for a residential building in Nanjing. The coefficient of performance (COP) of the system has increased by 11.22%, yielding to 24% energy savings, while the efficiency of the solar PVT system has improved by 11.8%. Moreover, Latorre-Biel et al.[17] have proposed a replacement of electric boilers and electric heat pump. They have studied three options: underfloor heating by a geothermal source, low-temperature radiators, and conventional radiators. They have found that air source heat pump with geothermal source have achieved more significant performance and less environmental impact than the other solutions. Also, Michopoulos et al.[18] investigated a system composed of geothermal water-water heat pump to provide heating and cooling loads for a residential house of 106.25 m^2 total floor area and solar collectors with an auxiliary boiler to provide domestic hot water. The proposed system reduced the total energy consumption by 54%.

Furthermore, thermal energy storage, which is known as thermal battery systems, can be utilized. A thermal battery device contains a material that stores thermal energy in the form of sensible thermal energy or latent thermal energy. Domestic hot water systems operated by solar systems are mostly stored as a sensible storage device, which needs a continuous, free of fluctuations thermal supply to efficiently perform. The best option is to use a phase-change thermal battery system, which counts on the latent thermal storage only. This type of system can store energy in a small amount compared to sensible thermal battery system and allow better control over the inlet collector fluid temperature. This is especially important for a PVT system since the solar cell temperature and the electrical performance strongly depends on the inlet fluid temperature to the PVT collectors.

For example, Zhang et al.[19] utilized a solar energy system with a phase-change thermal storage system. This system achieved full operation during the winter season in China and saved 40% of energy consumption. In addition, Tahersima et al.[20] designed a thermal battery system in a thick concrete flooring as a floor radiant heating system for a 3000 m^2 industrial facility. The radiant heating system was connected to a geothermal heat pump system. This system was able to provide a comfortable and sustainable indoor environment in the winter season due to the floor thermal storage with a lower operation cost. Also, O'Shaughnessy et al.[21] developed load control technologies for an integrated renewable energy system in a smart residential building. The proposed system is a combination of solar PVT system, thermal battery system, and control devices for lowering grid export rates and demand charges. Moreover, a smart grid optimized building was designed by Georgakarakos et al.[22] in order to adapt the required heating load between the thermal battery system and the electric demand from the electrical grid.

As a combination of solar energy and thermal storage energy, Beausoleil-Morrison et al.[23] presented a simulation of a full-scale residential building of 150 m^2 gross floor area located in Ottawa, Canada. The residential building is equipped with solar collectors (41.6 m^2), diurnal and seasonal thermal storage systems to provide thermal energy to radiant flooring system and domestic hot water. They found that the energy delivered by the total

thermal storage systems provided about 87% to 98% of the building heating load and thermal energy of the domestic hot water. The thermal efficiency of system during the diurnal and seasonal time was obtained to be 92% and 69%, respectively. In addition, Wills et al.[24] developed a simulation model for a similar system connected to a single-family detached dwelling of 132.3 m^2 gross floor area in Ottawa, Canada. There was no significant difference between the results from the new model and the measured results.

A similar study has been conducted in Thessaloniki, Greece.[25] Antoniadis and Martinopoulos constructed a system of solar collectors and a seasonal thermal storage tank to provide heating load and domestic hot water for a residential building of 120 m^2 gross floor area. It was found that the designed system can provide 67% of the total heating load required. However, an auxiliary system should be utilized during the extreme winter season in order to provide the total heating load of the building.

Most of the integrated systems have been studied as a combination of the solar system and heat pump system, with either a geothermal system or a thermal battery system. The combination of the four systems has not been investigated. Therefore, the purpose of this paper is to investigate the application of the hybrid system that combines a thermal battery system, a solar PVT system, and a GSHP system in order to achieve the following: reduce the utilization of fossil fuel furnaces, and provide reliable space heating, and long-period domestic hot water. The paper also presents a thermodynamic analysis including energy analysis and exergy analysis of the hybrid system for a residential building of 325 m^2 gross flooring area.

2 | SYSTEM DESCRIPTION

A hybrid renewable energy system consists of a latent-capable thermal battery of a 9463.53-kg (2500 gal) thermal battery that has three 700′ sections of 3/4′ poly pipe, piped in parallel inside the tank. Three of 3′ × 6.5′ flat solar thermal collectors were added and a flat plate heat exchanger in the primary/ drain-back loop was installed. One 300′ borehole was drilled for the sole "geo" capacity. The heat pump is a five-ton split system, which is installed beside the existing furnace and connected to the furnace by "F" coil. If the system was to become fully depleted or if something mechanical broke, the propane furnace could provide back-up heat.

Figure 1 illustrates the hybrid thermal battery system. The heat pump unit consists of a compressor (CM), an expansion valve (EX4), an evaporator (EV), and a condenser (CN). The heat exchanger or condenser (CN) is connected to a furnace unit by the furnace coil (F) to provide heating if the discharge coil (D) from the thermal

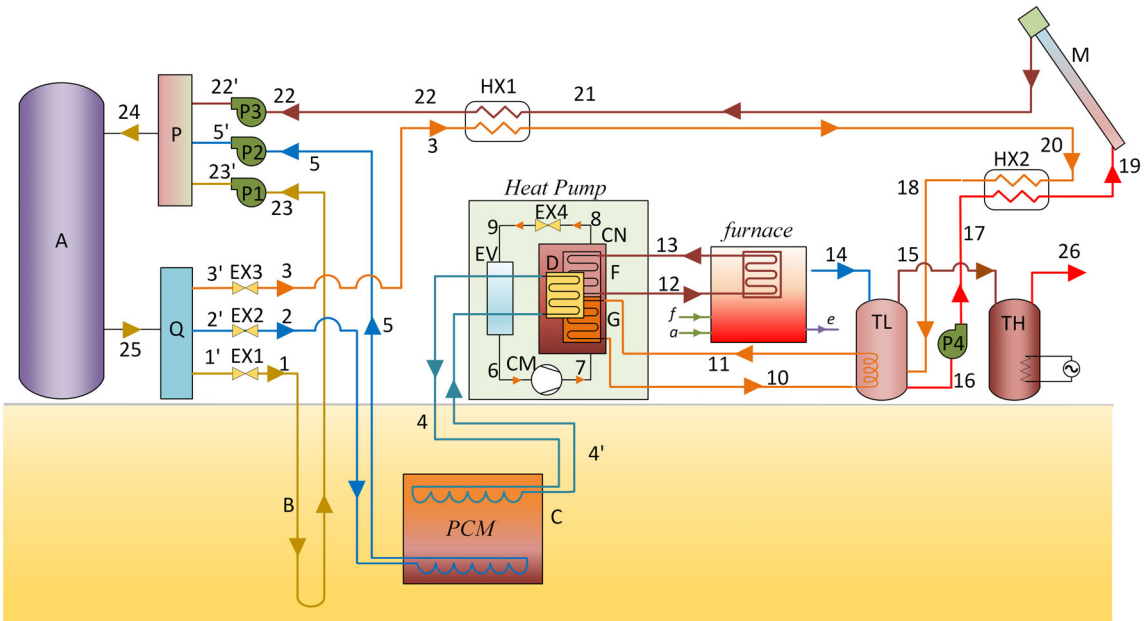

A- transfer tank
B- geothermal loop
C- thermal battery unit
F- furnace coil
I- furnace unit
EV- evaporator
CM- compressor
CN- condenser
EX- expansion valve
G- tank TL heating coil
D- discharge coil
TL- preheater water tank
TH- domestic hot water tank
HX1- high heat exchanger
HX2- low heat exchanger
M- solar collectors
O- high heat exchanger
P- collector unit
Q- distributor unit

FIGURE 1 A schematic diagram of the thermal battery system

battery unit (C) and geothermal loop (B) and the solar system unit (M) do not provide enough heating source during the extreme winter conditions. That means the only CN and the back-up furnace coil (F) will operator during shortage heating load. The furnace operates using a combustion chamber of burning liquid propane fuel (f) and air (a) while the products exit at (e) to the chimney of the building. The transfer tank (A) is connected to two units, as shown in the figure: a distributor unit (Q) and a collector unit (P). The first unit (Q) is used to deliver certain amounts to geothermal system (B), heat pump system, and PVT solar panels (M) through heat exchangers (HX1) and (HX2), while the latter unit (P) is used to collect the return flow from the geothermal unit (B), the thermal battery unit (C), and the solar collectors (M). There are two water tanks: preheated water tank (TL) which is connected to a heat exchanger (HX2) to heat the water exiting from the tank to the solar collector (M), while the domestic hot water tank (TH) collects the preheated water from the tank (TL) and heats it by the electric heater for the desired domestic hot water services.

A thermal battery storage does not discriminate between different sources of heat. The battery will accept heat from any source at the time it is available and rejects heat when it is abundant. It also collects and stores energy and provides a stabilizer during the maximum and minimum heating season. It consists of three main components: the charging coil that provides heat from the geothermal loop and PVT solar panels, the stored phase change material (PCM) fluid, which is selected to be water to store the heat; and the discharge coil that is connected to the condenser of heat pump as indicated by coil (D). The water in the thermal battery is chosen as a latent heating transfer fluid storage. it also helps resisting fully depletion of the hybrid system. That is because the temperature of the thermal battery will drop steadily as it enters the heating season until it drops down to freezing, then the temperature levels out at 0°C (32 °F), since the latent heat fusion of water is 333 kJ/kg. The heat pump continues to pull the required heat from the thermal battery, but it never turns to solid ice.

3 | SYSTEM ANALYSIS

The thermodynamic analysis consists of mass conservation, energy conservation, and exergy conservation as stated in the first and second laws of thermodynamics for each component and the whole system. The EES (Energy Equation Solver) software was selected because it is powerful engineering tool that solve thousands of coupled algebraic and differential equations and has a high accuracy thermodynamic and transport property database to provide all thermodynamic properties of used components in this research.[26,27]

Therefore, three conservation equations were studied including mass, energy, and exergy balance equations for each component and the entire system. The overall energy efficiency and exergy efficiency are also performed. The analyses are done based on several assumptions, which are listed as the following:

- All components and the entire system operate under steady state conditions.
- The reference environmental conditions are at reference temperature $T_o = 25°C$ and reference pressure $P_o = 101.325$ kPa.
- The heat losses from the system boundaries are negligible.
- The pressure losses are neglected through the pipeline connection, heat pump cycle, thermal battery, geothermal loop, and heat exchanger.

3.1 | Solar collector

The solar collector is the PVT solar panel type. It depends on the incident solar irradiance that generates a photocurrent source to generate the electrical power. The thermal part refers to the thermal change in the fluid stored in the solar collector since the solar panel surface is heated by the incident solar irradiance, which heats the flowing fluid.[28] Therefore, the energy analysis of PVT solar collector consists of thermal analysis and electrical analysis.

3.1.1 | Thermal analysis

Figure 2 shows the cross-sectional view of a PVT solar collector and the equivalent thermal resistors for each layer. The thermal analysis of PVT solar collector can be obtained by energy balance equation of each component of the solar panel,[29-31] consisting of the glass-absorber, the absorber plate, and the water flow in the pipes of PVT solar panels.

(1) Energy balance for glass-absorber PV module considers the incident solar radiation to the glass, which is transferred by conduction and convection heat mode to the solar cells and the absorber plate and generates the rate of electrical energy by the PV model, as shown in Figure 2. The energy balance can be described as Equation (1).

$$\tau_g \alpha_c \beta_c G_s DL = \left[U_t(T_c - T_a) + U_P\left(T_c - T_p\right)\right] DL + \tau_g \beta_c \eta_{el} G_s DL \quad (1)$$

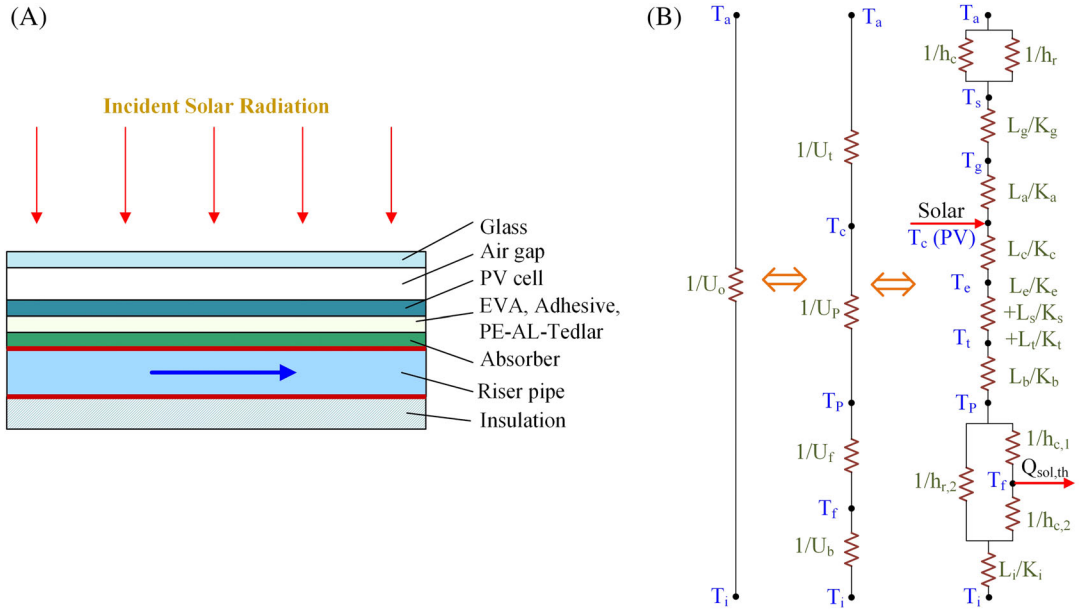

FIGURE 2 Cross-sectional view of PVT solar panel and the equivalent thermal resistors

where T_c, T_a, T_p, U_t, U_P, G_s, D, L, α_c, β_c, τ_g, and η_{el} are solar cells temperature, ambient temperature, absorber plate temperature, overall heat transfer coefficient from solar cell to the ambient through the glass, overall heat transfer from the cell to the absorber plate, solar radiation intensity, the width of absorber plate on a flow pipe, the length of solar panel, the absorptivity of solar cells, the packing factor of solar cells, the transmissivity of glass cover, and the electrical efficiency of the PVT module, respectively.

An expression for the solar cells temperature can be obtained as a function of ambient temperature T_a and absorber plate temperature T_p as shown in Equation (2)

$$T_c = \frac{\tau_g \beta_c (\alpha_c - \eta_{el}) G_s + U_t T_a + U_P T_P}{U_t + U_p} \tag{2}$$

(2) Energy balance for the absorber plate on a flow pipe describes the thermal energy transferred to the fluid, which is a function of the generation of electrical energy and the thermal energy from the cell to the absorber plate, as described in Equation (3)

$$\begin{aligned} U_f(T_p - T_f)DL &= \tau_g^2 \alpha_p (1-\beta_c) G_s DL + U_P(T_c - T_p) \\ DL &= \left[\tau_g^2 \alpha_p (1-\beta_c) + \tau_g \beta_c (\alpha_c - \eta_{el}) h_{p1}\right] G_s DL - U_{tp}(T_p - T_a) \end{aligned} \tag{3}$$

where U_f and α_p are the overall heat transfer of the flowing fluid and the absorptivity of the absorber plate. To simply Equation (3), the h_{p1} and U_{tp} are used as Equation (4) and (5) and defined as penalty factor and the overall heat transfer coefficient from glazing to the absorber plate from T_a and T_P, respectively, as shown in Figure 2.

$$h_{p1} = \frac{U_p}{U_t + U_p} \tag{4}$$

$$U_{tp} = \frac{U_t U_p}{U_t + U_p} \tag{5}$$

The absorber plate temperature can be obtained as a function of the absorbed solar radiation, electrical energy, ambient temperature T_a, and water flow temperature T_f, as shown in Equation (6)

$$T_P = \frac{\left[\tau_g^2 \alpha_p (1-\beta_c) + \tau_g \beta_c (\alpha_c - \eta_{el}) h_{p1}\right] G_s + U_{tp} T_a + U_f T_f}{U_{tp} + U_f} \tag{6}$$

An expression for the heat flux, which is transferred to the absorber plate, is obtained as in Equation (7):

$$\tau_g^2 \alpha_p (1-\beta_c) G_s + U_P(T_c - T_p) = (\alpha\tau)_{\text{eff}} G_s - U_{tf}(T_f - T_a) \tag{7}$$

where $(\alpha\tau)_{\text{eff}}$ is the product of effective absorptivity and transmissivity, h_{p2} is penalty factor, and U_{tf} is overall heat transfer coefficient from glazing to the fluid, which can be written as follows:

$$(\alpha\tau)_{\text{eff}} = \left[\tau_g^2\alpha_p(1-\beta_c) + \tau_g\beta_c(\alpha_c - \eta_{el})h_{p1}\right]h_{p2} \quad (8)$$

$$h_{p2} = \frac{U_f}{U_f + U_{tp}} \quad (9)$$

$$U_{tf} = \frac{U_{tp}U_f}{U_{tp} + U_f} \quad (10)$$

(3) Energy balance for water flow in a pipe is defined as the rate of heat transfer to the water in a flow pipe, and it can be determined as Equation (11).

$$\dot{Q}_{sol,th} = \dot{m}_{19}C_p(T_{21} - T_{19}) \quad (11)$$

where $\dot{m}_{19}$ and C_p are the inlet mass flow rate to the solar panel and the specific heat capacity of water, respectively. The water flow temperature can be determined as a function of the pipe length (x) as shown in Equation (12).

$$T_f(x) = \left(T_a + \frac{(\alpha\tau)_{\text{eff}}G_s}{U_o}\right)\left(1 - \exp\left(\frac{-bF'U_ox}{\dot{m}_{19}C_p}\right)\right) + T_{19}\exp\left(\frac{-bF'U_ox}{\dot{m}_{19}C_p}\right) \quad (12)$$

where U_o and F' are the overall heat transfer of the PVT collector to the environment and the flat plate collector efficiency, which is about 0.895,[32] respectively. The outlet temperature T_{21} is obtained from the previous equation with the boundary condition $T_f = T_{21}$, at $x = L$ as described in Equation (13).

$$T_{21} = \left(T_a - T_{19} + \frac{(\alpha\tau)_{\text{eff}}G_s}{U_o}\right)\left(\frac{F_RU_obL}{\dot{m}_{19}C_p}\right) + T_{19} \quad (13)$$

$$F_R = \frac{\dot{m}_{19}C_p}{U_obL}\left[1 - \exp\left(\frac{-bF'U_oL}{\dot{m}_{19}C_p}\right)\right] \quad (14)$$

where F_R and L are the heat removal factor and the length of the flow pipe, respectively. Also, b is the total width of the PVT solar collector.

The thermal efficiency of the PVT solar panel is defined as in Equation (15):

$$\eta_{sol,th} = \frac{\dot{Q}_{sol,th}}{G_sA} \quad (15)$$

3.1.2 | Electrical analysis

The four-parameter current-voltage (I-V) model is used to calculate the electrical parameters of PVT solar collector.[32] The photocurrent source i_{PV} can be describes as Equation (16).

$$i_{PV} = i_{light} - i_{sat}\left[\exp\left(\frac{qV_{cell}}{V_t}\right) - 1\right] \quad (16)$$

where i_{light} is the light current, i_{sat} is the reverse saturation current, V_{cell} is the voltage of the solar cell, which is equivalent to the ratio of the voltage of the solar system to the number of cells in one panel, V_t is the thermal voltage and is defined as $V_t = \gamma KT_{cell}/q$, where γ is the shape factor which is defined as $\gamma = a \times NCS \times N_s$, where a is the completion factor, NCS is the number of cells connected in series in a single module, N_s is the number of modules connected in series of the entire PV array, T_c is the surface temperature of the cell, which is defined below, q is the charge of a single electron, and ε_G is the electron band gap energy, which is 1.124 eV for mono-crystalline silicon modules. The light current, i_{light}, and reverse saturation current, i_{sat}, can be defined as (17) and (18).

$$i_{light} = i_{sc,ref}\left[1 + \Delta i_{sc}\left(T_c - T_{c,ref}\right)\right]\frac{G_s}{G_{ref}} \quad (17)$$

$$i_{sat} = i_{sat,ref}\left(\frac{T_c}{T_{c,ref}}\right)^3\exp\left[\left(\frac{q\varepsilon_G}{aK}\right)\left(\frac{1}{T_{c,ref}} - \frac{1}{T_c}\right)\right] \quad (18)$$

At the reference condition, the surface temperature of the solar cell, $T_{c,\ ref}$, is equivalent to 25°C, the reference solar intensity G_{ref} is equal to 1000 W/m^2. $i_{sc,\ ref}$ is the short circuit current of a single PV module under reference conditions, which is assigned by the manufacturer. At the reference condition, the short circuit current is almost equal to the light current ($i_{sc,\ ref} \approx i_{light,\ ref}$) and is a function of the open-circuit voltage at the reference condition, $V_{oc,\ c}$, which is defined by the manufacturer. Therefore, the reverse saturation current at the reference condition $i_{sat,\ ref}$ can be estimated as Equation (19).

$$i_{sat,ref} = \frac{i_{light,ref}}{\exp\left[\frac{V}{V_t}\right] - 1} \quad (19)$$

The power generated from the photovoltaic cells can be determined as the following:

$$\dot{W}_{sol} = N \times i_{PV} \times V \quad (20)$$

where V is the terminal voltage, which is a multiple of 12 V, and can be chosen to be 48 V, and N is the number of solar panels used in this study.

TABLE 1 Thermodynamic balance equations

Component	M.B.E [a]	E.B.E [b]	Ex.B.E [c]
Solar PV/T collector	$\dot{m}_{19}=\dot{m}_{21}$	Following section 3.1	$\dot{m}_{sol,in}ex_{19}+\left[1-\frac{4}{3}\left(\frac{T_o}{T_{sun}}\right)+\frac{1}{3}\left(\frac{T_o}{T_{sun}}\right)^4\right]\dot{Q}_{sol}$ $=\dot{m}_{sol,out}ex_{21}+\dot{W}_{sol}+\dot{E}x_{des,sol}$
Thermal battery	$\dot{m}_4=\dot{m}_5$	$\dot{m}_4h_4-\dot{m}_5h_5-\dot{Q}_{l,bat}=\dot{E}_{bat,f}-\dot{E}_{bat,i}$	$\dot{m}_4ex_4-\dot{m}_5ex_5-\left(1-\frac{T_o}{T_s}\right)\dot{Q}_{l,bat}-\dot{E}x_{des,bat}=\dot{E}x_{bat,f}-\dot{E}x_{bat,i}$
Geothermal loop	$\dot{m}_1=\dot{m}_{23}$	$\dot{m}_1h_1-\dot{m}_{23}h_{23}=\dot{E}_{geo,f}-\dot{E}_{geo,i}$	$\dot{m}_1ex_1-\dot{m}_{23}ex_{23}-\dot{E}x_{des,geo}$ $=\dot{E}x_{geo,f}-\dot{E}x_{geo,i}$
Furnace	$\dot{m}_{12}=\dot{m}_{13}$	$\dot{Q}_{fur}=\frac{\dot{m}_fQ_{out}}{M_f}=\dot{m}_{12}(h_{13}-h_{12})$	$\overline{Ex}_r=\overline{Ex}_p+\left(1-\frac{T_o}{T_s}\right)\dot{Q}_{fur}+\overline{Ex}_{des}$
Heat Pump			
1. Condenser	$\dot{m}_8=\dot{m}_7$	$\dot{Q}_{CN}=\dot{m}_7(h_8-h_7)$	$\dot{m}_7ex_7=\dot{m}_8ex_8+\left(1-\frac{T_o}{T_s}\right)\dot{Q}_{CN}+\dot{E}x_{des,CN}$
2. Evaporator	$\dot{m}_9=\dot{m}_6$	$\dot{Q}_{EV}=\dot{m}_9(h_9-h_6)$	$\left(\frac{T_o}{T_s}-1\right)\dot{Q}_{EV}+\dot{m}_9ex_9=\dot{m}_6ex_6+\dot{E}x_{des,EV}$
3. Compressor	$\dot{m}_6=\dot{m}_7$	$\dot{W}_{CM}=\dot{m}_6(h_7-h_6)$	$\dot{W}_{CM}+\dot{m}_6ex_6=\dot{m}_7ex_7+\dot{E}x_{des,CM}$
Expansion Valves	$\dot{m}_{EX,in}=\dot{m}_{EX,out}$	$h_{EX,\ in}=h_{EX,\ out}$	$\dot{m}_{EX,in}ex_{in}=\dot{m}_{EX,out}ex_{EX,out}+\dot{E}x_{des,EX}$
Pumps	$\dot{m}_{p,i}=\dot{m}_{p,o}$	$\dot{W}_p=\dot{m}_{p,i}(h_{p,o}-h_{p,i})$	$\dot{W}_p+\dot{m}_{p,i}ex_{p,i}=\dot{m}_{p,o}ex_{p,o}+\dot{E}x_{des,p}$
Distributor unit	$\dot{m}_{25}=$ $\dot{m}_1+\dot{m}_2+\dot{m}_3$	$\dot{m}_{25}h_{25}=\dot{m}_1h_1+\dot{m}_2h_2+\dot{m}_3h_3$	$\dot{m}_{25}ex_{25}=\dot{E}x_{des,Q}+\dot{m}_1ex_1+\dot{m}_2ex_2+\dot{m}_3ex_3$
Collector unit	$\dot{m}_{24}=$ $\dot{m}_{22}+\dot{m}_5+\dot{m}_{22}$	$\dot{m}_{24}h_{24}=\dot{m}_{22}h_{22}+\dot{m}_5h_5+\dot{m}_{22}h_{22}$	$\dot{m}_{24}ex_{24}+\dot{E}x_{gen,P}=\dot{m}_{22}ex_{22}+\dot{m}_5ex_5+\dot{m}_{22}ex_{22}$
Heat exchanger, O	$\dot{m}_{21}=\dot{m}_{22}$ $\dot{m}_3=\dot{m}_{20}$	$\dot{m}_{21}(h_{22}-h_{21})=\dot{m}_3(h_{20}-h_3)$	$\dot{m}_{21}ex_{21}+\dot{m}_3ex_3=\dot{m}_{20}ex_{20}+\dot{m}_{22}ex_{22}+\dot{E}x_{des,O}$
Heat exchanger, L	$\dot{m}_{20}=\dot{m}_{18}$ $\dot{m}_{17}=\dot{m}_{19}$	$\dot{m}_{20}(h_{18}-h_{20})=\dot{m}_{17}(h_{17}-h_{19})$	$\dot{m}_{17}ex_{17}+\dot{m}_{20}ex_{20}=\dot{m}_{18}ex_{18}+\dot{m}_{19}ex_{19}+\dot{E}x_{des,L}$
Preheater tank, TL	$m_f=m_i+(\dot{m}_{14}-\dot{m}_{15})t$	$\dot{Q}_G=\dot{m}_{14}(h_{10}-h_{11})$ $=\dot{m}_{18}(h_{16}-h_{18})$ $+\dot{m}_{15}h_{15}-\dot{m}_{14}h_{14}$ $+(m_fu_f-m_iu_i)t$	$\dot{Q}_G\left(1-\frac{T_o}{T_s}\right)+\dot{m}_{14}ex_{14}+\dot{m}_{18}ex_{18}=\dot{m}_{15}ex_{15}+\dot{m}_{16}ex_{16}+\dot{E}x_{des,TL}+(1/t)\left(m_fex_f-m_iex_i\right)$
Heater tank, TH	$m_f=m_i+(\dot{m}_{17}-\dot{m}_{26})t$	$\dot{W}_{TH}=\dot{m}_{17}h_{17}-\dot{m}_{26}h_{26}$ $+(m_fu_f-m_iu_i)t$	$\dot{W}_{TH}+\dot{m}_{17}ex_{17}=\dot{m}_{26}ex_{26}+\dot{E}x_{des,TH}+(1/t)\left(m_fex_f-m_iex_i\right)$
Transfer tank, A	$m_f=m_i$ $\dot{m}_{24}=\dot{m}_{25}$	$\dot{Q}_A=\left(m_fu_f-m_iu_i\right)t$	$\dot{E}x_{des,A}=(1/t)\left(m_iex_i-m_fex_f\right)$

[a]Mass balance equations [b] Energy balance equations [c] Exergy balance equations

The effective and maximum electrical efficiency of the PVT can be defined as Equations (21) and (22)

$$\eta_{el} = \frac{i_{PV} \times V}{G_s A} \tag{21}$$

$$\eta_{el,max} = \frac{i_{mp} \times V_{mp}}{G_s A} \tag{22}$$

In addition, the power ratio of the solar panel is determined as the ratio of the actual generated electrical power to the maximum electrical power of the PVT solar panel, as shown in Equation (23)

$$P_s = \frac{i_{PV} \times V}{i_{mp} \times V_{mp}} \tag{23}$$

The overall efficiency can be defined as shown in Equation (24)

$$\eta_{sol} = \frac{\dot{Q}_{sol,th} + i_{PV} \times V}{G_s A} \tag{24}$$

The mass, energy, and exergy balance equations are listed in Table 1. The energy and exergy efficiency of the system are also listed in Table 2.

TABLE 2 Energy and exergy efficiencies for each component

Component	η	ψ
Solar PV/T collector	$\frac{\dot{W}_{sol}+\dot{Q}_{sol,th}}{\dot{Q}_{sol}}$	$\frac{\dot{W}_{sol}+\dot{Q}_{sol,th}\left(1-\frac{T}{T_s}\right)}{\left[1-\frac{4}{3}\left(\frac{To}{T_{sun}}\right)+\frac{1}{3}\left(\frac{To}{T_{sun}}\right)^4\right]\dot{Q}_{sol}}$
Thermal battery	$\frac{\dot{Q}_{PCM,HP}}{\dot{Q}_{geo,PCM}}$	$\frac{\dot{Q}_{PCM,HP}\left(1-\frac{T}{T_{2,1}}\right)}{\dot{Q}_{geo,PCM}\left(1-\frac{To}{T_{s,2}}\right)}$
Geothermal loop	$\frac{\dot{m}_1 h_1}{\dot{m}_{23} h_{23}}$	$\frac{\dot{m}_1 ex_1}{\dot{m}_{23} ex_{23}}$
Furnace	$\frac{\dot{Q}_{out,I}}{\dot{m}_f HHV}$	$\frac{\left(1-\frac{T}{T_s}\right)\dot{Q}_{out,I}}{\dot{E}x_r}$
Heat Pump		
1. Condenser	$\frac{\dot{Q}_{CN}}{\dot{m}_7(h_8-h_7)}$	$\frac{\dot{m}_8 ex_8+\left(1-\frac{T}{T_S}\right)\dot{Q}_{CN}}{\dot{m}_7 ex_7}$
2. Evaporator	$\frac{\dot{m}_9(h_9-h_6)}{\dot{Q}_{EV}}$	$\frac{\dot{m}_6 ex_6}{\left(\frac{T}{T_s}-1\right)\dot{Q}_{EV}+\dot{m}_9 ex_9}$
3. Compressor	$\frac{h_{7,isen}-h_6}{h_7-h_6}$	$\frac{\dot{m}_6(ex_7-ex_6)}{\dot{W}_{CM}}$
Expansion Valves	$\frac{\dot{m}_{EX,out}h_{EX,out}}{\dot{m}_{EX,in}h_{EX,in}}$	$1-\frac{\dot{E}x_{des,EX}}{\dot{m}_{EX,in}ex_{EX,in}}$
Pumps	$\frac{h_{p,o,isen}-h_{p,i}}{h_{p,o}-h_{p,i}}$	$1-\frac{\dot{E}x_{des,p}}{\dot{m}_{p,i}ex_{p,i}+\dot{W}_p}$
Distributer unit	$\frac{\dot{m}_1h_1+\dot{m}_2h_2+\dot{m}_3h_3}{\dot{m}_{25}h_{25}}$	$1-\frac{\dot{E}x_{des,Q}}{\dot{m}_{25}ex_{25}}$
Collector unit	$\frac{\dot{m}_{24}h_{24}}{\dot{m}_{22}h_{22}+\dot{m}_5h_5+\dot{m}_{22}h_{22}}$	$1-\frac{\dot{E}x_{des,P}}{\dot{m}_{22}ex_{22}+\dot{m}_5ex_5+\dot{m}_{22}ex_{22}}$
Heat exchanger, O	$\frac{h_{22}-h_{21}}{h_{20}-h_3}$	$1-\frac{\dot{E}x_{des,O}}{\dot{m}_{21}ex_{21}+\dot{m}_3ex_3}$
Heat exchanger, L	$\frac{h_{18}-h_{20}}{h_{17}-h_{19}}$	$1-\frac{\dot{E}x_{des,L}}{\dot{m}_{17}ex_{17}+\dot{m}_{20}ex_{20}}$
Tank, TL	$\frac{(\dot{m}_{14}h_{14}-\dot{m}_{15}h_{15})}{\dot{Q}_G}$	$\frac{(\dot{m}_{14}ex_{14}-\dot{m}_{15}ex_{15})}{\dot{Q}_G\left(1-\frac{T}{T_s}\right)}$
Tank, TH	$\frac{(\dot{m}_{17}h_{17}-\dot{m}_{26}h_{26})}{\dot{W}_{TH}}$	$\frac{(\dot{m}_{17}ex_{17}-\dot{m}_{26}ex_{26})}{\dot{W}_{TH}}$
Transfer tank, A	$\frac{h_{25}}{h_{24}}$	$1-\frac{\dot{E}x_{des,A}}{\dot{m}_{24}ex_{24}}$

3.2 | Thermal battery storage

The thermal battery involves temporary storage of high- or low-temperature thermal energy for later use. The thermal battery storage process is closed tank storage with two heat exchangers and is composed of three subprocesses: charging, storing, and discharging. For overall process, the thermodynamic analysis is considered to be in an equilibrium state, where a charging state (state 4 in Figure 1) and a discharging state (state 5 in Figure 1) are considered. The overall energy balance of the PCM thermal battery storage is written as Equation (25)

$$\dot{Q}_{geo,PCM} - \left(\dot{Q}_{PCM,HP} + \dot{Q}_{PCM,loss}\right) = \frac{\Delta E_{PCM,stored}}{\Delta t} \tag{25}$$

where $\dot{Q}_{geo,PCM}$ is the heat transfer from the transfer tank to the thermal battery storage, $\dot{Q}_{PCM,HP}$ is the heat transfer from the thermal battery to the heat pump, $\dot{Q}_{PCM,loss}$ is the heat loss or gain from the soil over the year, and $\Delta E_{PCM,\ stored}$ is the stored energy of the PCM, which can be defined as Equation (26)

$$\Delta E_{PCM,stored} = \rho_w V_{PCM}\left(u_f - u_i\right) \tag{26}$$

where u_i and u_f refer to the internal energy of the initial and final state of the stored water in the thermal battery storage, which may contain two phases, that is, solid (some ice) and liquid phase at 0°C. Therefore, the stored energy can be described as follows:

$$\Delta E_{PCM,stored} = m_{PCM} cp_{ice} \Delta T + mL_f + m_{PCM} cp_w \Delta T \tag{27}$$

The heat loss or gain form the soil can be explained as Equation (28):

$$\dot{Q}_{PCM,loss} = A_{PCM,sur} K_{soil} \frac{\Delta T}{\Delta z} \tag{28}$$

where $A_{PCM,sur}$ is the total surface area of the storage tank of six sides, K_{soil} is the thermal conductance of the soil, and $\Delta T/\Delta z$ is the temperature gradient below 5 m under the ground surface.

The energy balance of the PCM thermal battery system can be divided into three section: charging, storing, and

discharging energy. The charging fluid is the water flow from the transfer tank to the thermal battery, while the discharging fluid describes the water flow from the thermal battery to the heat pump. The charging period is when charging fluid is used for heating the PCM storage fluid, which will be stored in the PCM fluid for a period of time and then will be used for heating the discharge fluid. Therefore, the energy balance equation for the charging period can be described as Equation (29) and (30)

$$\dot{Q}_{geo,PCM} - \dot{Q}_{PCM,loss,1} = \frac{\Delta E_{PCM,1}}{\Delta t_c} \tag{29}$$

$$\dot{m}_2(h_2 - h_5) - \dot{Q}_{PCM,loss,1} = \frac{m_{PCM} cp_w (T_{f,1} - T_i)}{\Delta t_c} \tag{30}$$

The energy balance equation for the storing period can be written as Equation (31):

$$-\dot{Q}_{PCM,loss,2} = \frac{\Delta E_{PCM,1}}{\Delta t} = \frac{m_{PCM} cp_w (T_{f,2} - T_{f,1})}{\Delta t_s} \tag{31}$$

The energy balance equation for the discharging period can be given as Equations (32) and (33).

$$-\left(\dot{Q}_{PCM,HP} + \dot{Q}_{PCM,loss,3}\right) = \frac{\Delta E_{PCM,3}}{\Delta t_d} \tag{32}$$

$$-\left[\dot{m}_4(h_{4'} - h_4) + \dot{Q}_{PCM,loss,3}\right] = \frac{m_{PCM} cp_w (T_{f,3} - T_{f,2})}{\Delta t_d} \tag{33}$$

where Δt_c, Δt_s, and Δt_d are the charging, storing, and discharging periods, respectively. $\dot{Q}_{PCM,loss,1}$, $\dot{Q}_{PCM,loss,2}$, and $\dot{Q}_{PCM,loss,3}$ are the heat loss of the thermal battery to the soil, which are assumed to be equal for each period. Also, T_i is the initial temperature of the PCM fluid, while $T_{f,1}$, $T_{f,2}$, and $T_{f,3}$ are the PCM fluid temperature at the end of charging, storing, and discharging period, respectively. The mass, energy, and exergy balance equations are listed in Table 1. The energy and exergy efficiency of the system are also listed in Table 2.

3.3 | Geothermal loop

The geothermal loop (B in Figure 1) consists of a production flow to provide hot water flow to the hybrid system and a reinjecting flow to return the collected water back to the ground. The geothermal loop is buried vertically up to 300′ under the ground. The heat from the soil does not change dramatically as the climate change. It is a useful source of stable heat during the year. Neglecting the kinetic and potential energy changes, the energy balance of the geothermal loop can be written as Equation (34)

$$\dot{Q}_{geo} = \dot{m}_1(h_{23} - h_1) = \dot{m}_2 cp(T_{23} - T_1) \tag{34}$$

where $\dot{Q}_{geo}$ is the geothermal heat transfer, which will equal to heat transfer, and T_1 and T_{23} are the inlet and exit temperature of the geothermal loop. The temperature difference between the exit and inlet is 20°C and is assumed to be constant over the year due to the heat transfer from the soil to the geothermal loop. The mass, energy, and exergy balance equations are described in Table 1, while the energy and exergy efficiency of the geothermal loop are listed in Table 2.

3.4 | Furnace

Assuming the nontheoretical combustion process, the mass balance equation is expressed as the following:

$$\dot{m}_e = \dot{m}_a + \dot{m}_f \tag{35}$$

where $\dot{m}_a$ and $\dot{m}_f$ are defined as mass flow rate of air and propane fuel, while $\dot{m}_e$ is the mass flow rate of the exhaust product. The air-fuel ratio is defined based on mass as Equation (36).

$$AF = \frac{m_a}{m_f} = \frac{(NM)_a}{(NM)_C + (NM)_H} \tag{36}$$

Since the fuel is selected to be propane C_3H_8, which has a molar mass M_f of 44 kg/kmol, which is composed of the mass of carbon and mass of hydrogen, and the molar mass of air is equivalent to 28.97 kg/kmol. The ideal combustion process is when the fuel is completely burned with stoichiometric air in the theoretical combustion process. Therefore, the theoretical combustion process of propane is expressed as Equation (37).

$$C_3H_8 + a_{th}(O_2 + 3.76\,N_2) \rightarrow 3\,CO_2 + 4\,H_2O + 3.76 a_{th} N_2 \tag{37}$$

For balancing the oxygen, the stoichiometric amount of air a_{th} is estimated to be 5. Assuming an actual combustion process with 50% excess air and some CO in the products. Therefore, the actual combustion reaction will be:

$$\begin{aligned} C_3H_8 + 7.5\,(O_2 + 3.76\,N_2) \rightarrow\ & 2.7\,CO_2 + 0.3\,CO \\ & + 4\,H_2O + 2.65\,O_2 + 28.2\,N_2 \end{aligned} \tag{38}$$

Therefore, the air-fuel ratio for this combustion process is estimated to be 25.53 kg_a/kg_f. The combustion

chamber is considered to be a steady-flow system, so the energy balance equation of a chemically reacting steady-flow system can be expressed as Equation (39):

$$Q_{fur} = \sum N_r \left(\bar{h}_f^o + \bar{h} - \bar{h^o}\right)_r - \sum N_p \left(\bar{h}_f^o + \bar{h} - \bar{h^o}\right)_p \quad (39)$$

where N_r and N_p are the number of moles for each chemical reactant r and each chemical product p, respectively. $\bar{h}_f^o$, $\bar{h}$, and $\bar{h^o}$ are defined as the specific molar enthalpy formation, specific molar enthalpy at reaction temperature, and specific molar enthalpy at the standard conditions, respectively. This heat is used to heat the water circulated to the heat pump during the shortage of other resources. The heat of the furnace is also defined as Equation (40):

$$\dot{Q}_{fur} = \frac{\dot{m}_f Q_{fur}}{M_f} = \dot{m}_{12}(h_{13} - h_{12}) \quad (40)$$

The mass, energy, and exergy balance equations are explained in Table 1. The energy and exergy efficiency of the system are also written in Table 2. For the component i of an ideal-gas mixture, this relation can be written as Equation (41).

$$\bar{s}_i(T, P_i) = \bar{s}_i^o(T, P_o) - R_u \ln \frac{y_i P_m}{P_o} \quad (41)$$

where $\bar{s}_i^o$ is the absolute entropy per mole for each substance at $P_o = 1$ atm and temperature T, P_i is the partial pressure, which is equal to $P_i = y_i P_m$, y_i is the mole fraction of the component, and P_m is the total pressure of the mixture. While the exergy balance equation is composed of the molar exergy of reactants $\bar{Ex}_r$ and products $\bar{Ex}_p$ and thermal exergy $\bar{Ex}_Q$ as Equation (42):

$$\bar{Ex}_r = \sum_i N_{i,r}\left(\bar{g}_f^o + \bar{g} - \bar{g}^o\right)_r \text{ and } \bar{Ex}_p = \sum_i N_{i,p}\left(\bar{g}_f^o + \bar{g} - \bar{g}^o\right)_p \quad (42)$$

where $\bar{g}_f^o$, $\bar{g}$, and $\bar{g}^o$ are defined as the Gibbs function of formation, the Gibbs function of a substance at reaction temperature and the Gibbs function at standard conditions per unit mole, respectively. The Gibbs function per unit mole for a substance can be defined as $\bar{g}_i = \bar{h}_i - T_o \bar{s}_i$ as a function of specific molar enthalup and entropy.

3.5 | Heat pump

The heat pump consists of a compressor, a condenser, an expansion valve, and an evaporator. The condenser of the heat pump is combined with a back-up condenser unit from the furnace and a condenser of thermal battery unit (unit D in Figure 1) to guarantee the operation stability of the heat pump. The mass, energy, and exergy balance equations are listed in Table 1 for each component, while the energy and exergy efficiency of the system are also listed in Table 2.

The fan is used to deliver the hot air to a building for heating during the winter season. The total transferred heat to the air is a combination of the heat from the condenser of heat pump ($\dot{Q}_{CN}$), the heat from the back-up condenser ($\dot{Q}_{fur}$), and thermal battery condenser ($\dot{Q}_D$)

TABLE 3 Building Specifications

Building Specifications	Value
Floor area	72.25 m^2
Number of floors	3 floors including a basement
Average ceiling height	2.7 m
Building weight	405.2 kg/m^2 (medium)
Ventilation for the building	2.5 L/s/person
Number of residents	12 persons
Walls area	168.86 m^2 (RSI = 4.1 m^2.K/W)
Glass area	32.64 m^2 (RSI = 0.33 m^2.K/W)
Door area	2.5 m^2 (RSI = 1.703 m^2.K/W)
Roof area	72.25 m^2 (RSI = 6.7 m^2.K/W)
Basement wall area	88.4 m^2 (RSI = 3 m^2.K/W)

TABLE 4 Weather specifications of the city of Oshawa

Specification		Value
Latitude [°]		43.9
Longitude [°]		79.4 W
Altitude [m]		198
Climate Zone		5A - Cold Humid
Winter Season	Heating design temperature [°C]	-17.2
	Ambient Temperature [°C]	-5.5
	Relative humidity [%]	74.6
	Daily solar radiation-horizontal [MJ/m^2/d]	5.54
	Heating Degree Days [HDD]	729
Summer Season	Cooling design temperature	29.8
	Ambient Temperature [°C]	21.4
	Relative humidity [%]	68.5
	Daily solar radiation-horizontal [MJ/m^2/d]	21.1
	Cooling Degree days [CDD]	353

Source: RETScreen software.[34]

TABLE 5 Specification of the hybrid system

Element	Value
Solar panels type:	PV/T type TESZEUS 300M [36,37]
External dimensions (mm)	1956 x 992 x 50
Thermal Absorber material	Copper/Aluminum
Peak Power (pm)	300
Open Circuit (V_{oc})	44.53 V
short circuit (I_{sc})	8.9 A
Maximum power voltage (V_{mp})	37.1 V
Maximum power current (I_{mp})	8.09 A
Cell efficiency	17.35%
Panel efficiency	15.54%
loss factor P_{max} (%/K)	0.4%
Working Temperature	-40 ^{0}C to +85^{0}C
Tolerance	±3%
Thermal battery capacity	9463.53 kg of water (size: 4.04m x 2.51m x 1.3m)
Water as PCM [38]	
Melting point	0 ^{0}C
Latent heat of fusion (L_f)	333 kJ/kg
Density (solid phase) (ρ_{ice})	900 kg/m^3,
Specific heat (solid phase) (cp_{ice})	2.09 kJ/kg.K,
Thermal conductivity (solid phase) (K_{ice})	2.2 W/m.k
Density (liquid phase) (ρ_w)	1000 kg/m^3 (at 0 ^{0}C)
Specific heat (liquid phase) (cp_w)	4.22 kJ/kg.K (at 0 ^{0}C) and 4.18 kJ/kg.K (at 25 ^{0}C)
Thermal conductivity (liquid phase) (K_w)	0.609 W/m.K
Heat pump capacity	5 ton
Geothermal loop capacity	11356.24 kg of water (length: 300 m)
Storage time	1 day

subtracting the heat for hot water services ($\dot{Q}_{TL}$), as shown in the following equation.

$$\dot{Q}_{air} = \dot{m}_{air}(h_{27} - h_{28}) = \dot{Q}_{CN} - \dot{Q}_{TL} + \dot{Q}_{fur} + \dot{Q}_D \quad (43)$$

During the summer season, the absorbed heat by the evaporator (*EV*) is used for cooling the building. Therefore, the thermal energy of the supply air in the summer can be defined as Equation (44):

$$\dot{Q}_{air} = \dot{Q}_{EV} \quad (44)$$

The COP of the heat pump (COP_{HP}) is defined as the ratio of the energy output to the compressor power of the heat pump, $\dot{W}_{CM}$. Therefore, the energetic $COP_{HP,en}$ and the exergetic $COP_{HP,ex}$ is defined as Equation (45):

$$COP_{HP,en} = \frac{\dot{Q}_{air}}{\dot{W}_{CM}} \text{ and } COP_{HP,ex} = \frac{\left(1 - \frac{T}{T_s}\right)\dot{Q}_{air}}{\dot{W}_{CM}} \quad (45)$$

3.6 | Distributor unit and collector unit

The distributor unit (Q) and the collector unit (P) can be studied as a mixing chamber that has multiple inlet flow rate with different thermodynamic properties and multiple exit flow rates. The mass, energy, and exergy balance equations are explained in Table 1. The energy and exergy efficiency of the system are also written in Table 2.

3.7 | Heat exchanger

Two heat exchangers are used in the hybrid system. One heat exchanger (HX2) is located between the preheat water tank (TL) and a solar collector, while the other (HX1) is located between the solar collector and the collector unit (P). Both heat exchangers are exchanging heat from a line that is coming from the transfer tank (A) directly to the tank (TL). Following the same thermodynamic principles, the mass, energy, and exergy balance equations are written in Table 1, while the energy and exergy efficiency of the system are in Table 2.

3.8 | Overall efficiencies

The energy and exergy inputs to the system are considered to be incident solar irradiance $\dot{Q}_{sol}$, the compressor power $\dot{W}_{CM}$, the summation of all pump powers, the energy rate of the cold water to Tank J, and change in energy rate of both geothermal and thermal battery systems, while the energy and exergy output elements are the solar power $\dot{W}_{sol}$, the hot air to the building $\dot{Q}_{air}$, and the energy rate of the hot water from the domestic hot water tank. Therefore the overall energetic COP of the entire system is defined as Equation (46):

$$COP_{sys,en} = \frac{\dot{W}_{sol} + \dot{Q}_{air} + \dot{E}_{26}}{\dot{Q}_{sol} + \dot{W}_{CM} + \sum \dot{W}_P + \dot{Q}_{geo} + \dot{Q}_{geo,PCM} + \dot{E}_{14}} \quad (46)$$

while the exergetic COP of the entire system is defined as Equation (47):

$$COP_{sys,ex} = \frac{\dot{W}_{sol} + \left(1 - \frac{T}{T_s}\right)\dot{Q}_{air} + \dot{E}x_{26}}{\left[1 - \frac{4}{3}\left(\frac{T_o}{T_{sun}}\right) + \frac{1}{3}\left(\frac{T_o}{T_{sun}}\right)^4\right]\dot{Q}_{sol} + \dot{W}_{CM} + \sum \dot{W}_P + \Delta\dot{E}x_{geo} + \Delta\dot{E}x_{geo,PCM} + \dot{E}x_{14}} \quad (47)$$

3.9 | Component exergy destruction

The energy destruction of each component is defined previously in each section; the total energy destruction can be expressed as Equation (48):

$$\dot{E}x_{des,total} = \sum_i \dot{E}x_{des,i} \quad (48)$$

and the irreversibility ratio for each component can be defined as Equation (49):

$$IR = \frac{\dot{E}x_{des,i}}{\dot{E}x_{des,total}} \quad (49)$$

4 | RESULTS AND DISCUSSION

Note that the present system is applied for a residential building with three floors each of 72.52 m^2 flooring area. The number of residents is 12 persons. The building specifications are listed in Table 3. The cooling and heating load of the building are estimated using Hourly Analysis Program HVAC System Design Software, known as Carrier HAP software version 4.9.[33] The Oshawa weather is classified as 5A-cold humid and obtained from the RETScreen software[34] as listed in Table 4. The thermodynamic properties and analysis were obtained using the EES software[26] for the entire system and the transient analysis of thermal storage. The hybrid system contains five major elements: solar panels, heat pump, geothermal loop, thermal battery storage, which their specifications are listed in Table 5.

The air temperature, wind velocity, and solar radiation is plotted in Figure 3. The maximum ambient temperature is 22°C in July, while the minimum ambient temperature is −5.5°C in January. The range of wind speeds is between 3 and 4 m/s. Also, the maximum and minimum solar incident radiation are 250 (in July) and 55 (in December) W/m^2, respectively.

The manufacture of PVT solar panel does not provide details of the design and materials used, such as different layers and their thermal properties and geometrical specifications, as shown in Figure 2. The optical and thermal properties of each layer are listed in Table 6. The overall heat transfer coefficients that mentioned in Section 3.1.1 are calculated in Table 7. The total overall of the PVT solar panel, U_o, is estimated to be 0.967 W/m^2 K.

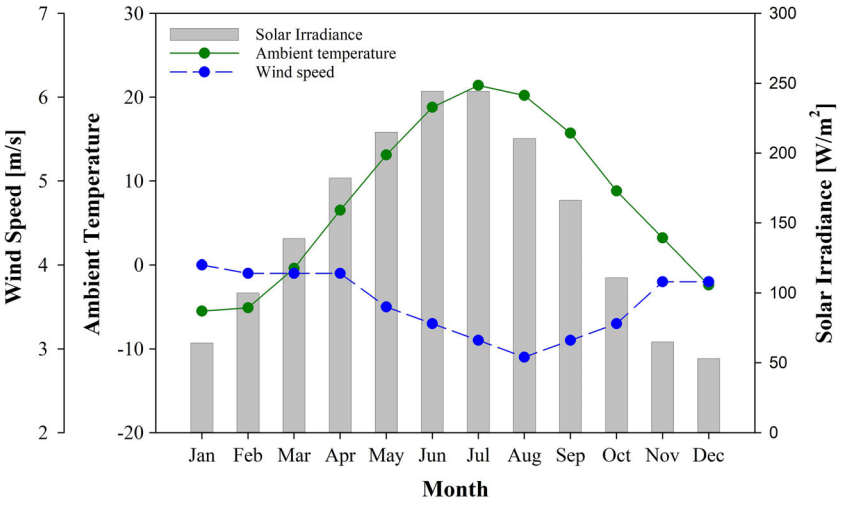

FIGURE 3 Weather conditions for Oshawa city, Canada

TABLE 6 The specifications of solar panel layers [30,39,40]

Layer			Value	Units
Glazing	A	Aperture area	1.94	m^2
	L_g	Thickness	0.0032	m
	ε_g	Emissivity	0.88	—
	τ_g	Transmittance	0.9	—
	ρ_d	Diffuse reflectance	0.16	—
	K_g	Thermal conductivity	1	W/m.K
Air layer	L_a	Thickness	0.005	m
	K_a	Thermal conductivity	0.025	W/m.K
PV Silicon Plate	A_{PV}	Area of the cell	1.94	m^2
	P	Covering factor	0.75	—
	β_c	Packing factor	0.9	—
	α_c	Absorptivity	0.9	—
	ε_c	Emissivity	0.9	—
	L_{si}	Thickness	350e-6	m
	K_{si}	Thermal conductivity	148	W/m.K
EVA	L_e	Thickness	0.0005	m
	K_e	Thermal conductivity	0.35	W/m.K
Adhesive	L_s	Thickness	0.00005	m
	K_s	Thermal conductivity	0.85	W/m.K
PE-AL-Tedlar Layer	L_t	Thickness	0.0001	m
	K_t	Thermal conductivity	0.2	W/m.K
Absorber plate	α_P	Absorptivity	0.95	—
	ε_P	Emissivity	0.05	—
	L_P	Thickness	0.002	m
	K_P	Thermal conductivity	310	W/m.K
Riser Tubes	D	Diameter of tube	0.01	m
	N	No. of tubes	11	—
	W	Spacing of tubes	0.095	—
Insulation	L_i	Thickness	0.02	m
	K_i	Thermal conductivity	0.035	W/m.K
PVT dimensions	L	PVT length	1.956	m
	D	PVT width	0.8	m
	L_{ch}	Characteristic length = 4A/P	1.136	m

TABLE 7 The overall heat transfer coefficients for a group of PVT layers

U-Parameters	Values ($W/m^2.K$)	U-Parameters	Values ($W/m^2.K$)
U_t	4.951	U_{tf}	4.856
U_P	15.5e4	U_{tp}	4.951
U_f	254.406	U_o	0.967
U_b	1.207		

The thermal properties of air spacing locating after the glass is stated in Table 8. Heat is transferred from the glass cover by convection or conduction through the air gap to the PV laminate. The convective heat transfer coefficient can be estimated by the Nusselt number ($Nu = h_c D_h/K$), which can be determined by the Grashof number $\left(Gr = g\cos\theta\beta_{air}\Delta T L_a^3/v_{air}^2\right)$.[40] The Gr is estimated to be 270 and therefore, the Nu is given to be 0.811 which 4 orders of magnitude lower than that of the convective heat mode ($Nu \approx 10^4$-10^7). Therefore, the natural convection in the air spacing is negligible, and the assumption

of conduction heat transfer of the air gap is reasonable,[40] as shown in Table 8.

The cooling and heating load of the building are obtained from carrier HAP software and presented in Figure 4. The maximum heating load is 13.8 kW in January, while the maximum cooling load is 8.68 kW in July. The designed building condition is set to be 20°C in the summer season and 27°C in the winter season. The supply air temperature is 18°C and 25°C in the summer and winter season, respectively.

The thermodynamic properties for each state points of Figure 1 are presented in Table 9 based on the winter season in January since the purpose of this hybrid system is to provide heating and hot domestic water. The heat transfer, produced or required work, exergy destruction, the irreversibility rate, the thermal efficiency, and exergetic efficiency are presented for each component in Table 10. The expansion valve (EX1) and the tank (TH) have the maximum value of the irreversibility rates (14.88% and 49.27%, respectively) because of high temperature difference to the environment. The total exergy rate of the cycle is 12.554 kW. The overall energetic and exergetic COP of the whole system is estimated to be 54.58% and 3.34%, respectively.

The building is heated by all the condenser coils consisting of a condenser, a thermal battery coil (D), and furnace coil (F). The Coil G is used to heat the preheated water tank (TL) by extracting heat from the condenser to heat the water in the preheated tank (TL). The values of heat transfer of all coils in the condenser is described in Figure 5. The total heat of the condenser including the furnace heat, is estimated to be 13.8 kW to be equivalent to the maximum heating load of the building.

The power and the heat transfer of the components in the system is plotted in Figure 6. The highest power consumption is 6.42 kW for electric heating used in the domestic hot water tank (TH). The condenser power consumption is evaluated as 2.15 kW. The power supplied from the PVT is 0.05 W for using five panels, while the thermal heating to the water in the PVT pipes is determined to be 0.008 kW (8 W) to raise the flow temperature from 29.13°C to 29.18°C because of the minimum incident solar radiation in the winter season. In addition, the integrated system can provide the total heating load equivalent to 13.8 kW, an energy rate of the domestic hot water to be 7.542 kW, and heat rejection by the evaporator of 9.485 kW that effectively can be used in cooling the building in the summer season.

The operation of the system started in July to gain the heat from the underground and the maximum solar irradiance to have better performance. Also, the system installation is preferred to be in spring and summer time to avoid digging in the ground covered with snow and ice. The PVT solar panels are used to heat the water flow and produce electricity by solar radiation. The inlet and exit temperatures of water flow rate ranges from 17°C to 27°C but increased by 0.05°C to 1°C, as shown in Figure 7A. The large temperature difference occurs in July, while the small difference occurs in January. The supply power ranges from 0.05 to 0.48 kW, and the thermal heat transfer varies between 0.003 and 0.29 kW, as illustrated in Figure 7B. In addition, the energetic efficiency varies from 12% to 31%, while the exergetic efficiency ranges from 12% to 21%, as shown in Figure 7C (Figure 8). In Figure 8, the energetic efficiency of PVT system comprises of thermal efficiency due to the themal heating of fluid flow and the electrical efficiency due to the electrical power of solar panels. The thermal effieciency varies from 3% in the winter to 11% in the summer, while the electrical efficiency has small variation at 21% over the year. However, the combination of both electrical and thermal

TABLE 8 The thermal properties of air space in the PVT solar panels

Parameter		Value	Unit
Air temperature	T_a	290	K
Inclination angle of solar panels	θ	60	o
Grashof no.	Gr	270	—
Rayleigh no.	Ra	1.92E+02	—
Prandtl no.	Pr	1.005	—
Nusselt no.	Nu	0.811	—
Convective heat transfer of air	$h_{a,gap}$	0.017	$W/m^2.K$

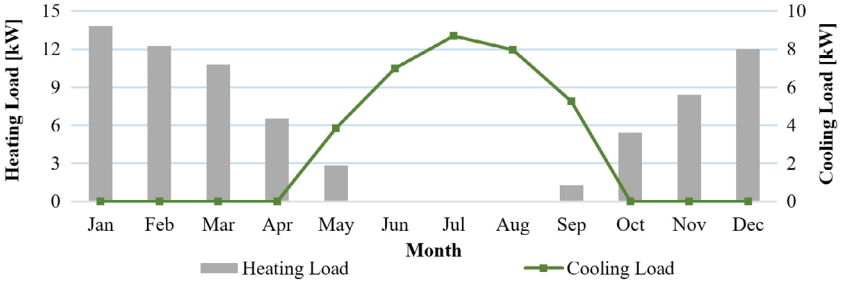

FIGURE 4 The heating and cooling load of the building in Oshawa city

TABLE 9 Thermodynamic properties of each state point in month of January

State	Description	fluid	$\dot{m}$ [kg/s]	T [^{0}C]	P [kPa]	h [kJ/kg]	s [kJ/kg.K]	ex [kJ/kg]
w0	Reference state	water		25	101.325	104.8	0.3669	—
r0	Reference state	R134a		25	101.325	276.4	1.105	—
a0	Reference state (φ = 50%)	Air		25	101.325	50.34	5.788	—
amb	Ambient air (φ = 74.6%)	air	0.2084	-5.5	101.325	9.751	5.644	-0.2944
1’	Inlet to EX1	Water	0.2	27	800	113.9	0.3947	0.7327
1	Inlet to geothermal loop	Water	0.2	27.09	400	113.9	0.396	0.3343
2’	Inlet to EX2	water	0.2	27	800	113.9	0.3947	0.7327
2	Inlet to PCM coil	water	0.2	27.09	400	113.9	0.396	0.3343
3’	Inlet to EX3	water	0.1	27	800	113.9	0.3947	0.7327
3	Inlet to HX1	water	0.1	27.11	300	113.9	0.3964	0.2347
4	Coil D Exit to PCM	water	0.18	12.09	400	51.12	0.1817	1.476
4’	PCM exit to coil D	water	0.18	24.09	400	101.3	0.354	0.3034
5	PCM exit to P2	water	0.2	15.09	400	63.67	0.2254	0.9831
5’	P2 exit to collector unit	water	0.2	15.13	800	64.24	0.226	1.378
6	Inlet to CM	R134a	0.07	5.008	350	253.3	0.9288	29.5
7	CM exit	R134a	0.07	55	1200	284	0.9444	55.52
8	CN exit	R134a	0.07	46.29	1200	117.8	0.4244	44.31
9	EX4 exit	R134a	0.07	5.008	350	117.8	0.4414	39.24
10	Coil G exit	water	0.07	50	400	209.7	0.7036	4.452
11	Inlet to Coil G	water	0.07	20	400	84.21	0.2961	0.4769
14	Inlet to tank TL	water	0.07	10	300	42.28	0.1509	1.801
15	Exit from tank TL	water	0.04	30	300	125.9	0.4364	0.3831
16	Inlet to P4	water	0.1	25.11	300	105.5	0.3684	0.1996
17	Exit from P4	water	0.1	25.13	500	105.8	0.3687	0.4002
18	From HX2 to tank TL	water	0.1	19.11	300	80.39	0.2834	0.4333
19	Inlet to solar panels	water	0.1	29.13	500	122.5	0.4244	0.5186
20	Inlet to HX2	water	0.1	23.11	300	97.12	0.3403	0.2204
21	Inlet to HX1	water	0.1	29.18	500	122.7	0.425	0.521
22	HX1 exit to P3	water	0.1	33.22	500	139.4	0.4806	0.6816
22’	P3 exit to collector unit	water	0.1	33.28	800	140.1	0.4813	1.19
23	Geothermal exit to P1	water	0.2	47.09	400	197.5	0.6657	3.605
23’	P1 exit to collector unit	water	0.2	47.14	800	198.1	0.6663	4.022
24	Inlet to transfer tank	water	0.5	31.57	800	132.9	0.4578	1.012
25	Transfer tank exit	water	0.5	27	800	113.9	0.3947	0.7327
26	hot domestic water outlet	water	0.03	60	300	251.4	0.831	8.241
27	Outdoor air	air	0.2084	-17.2	101.3	-15.88	5.548	5.149
28	Supply air to the room	air	0.2084	25	101.3	50.34	5.788	0

efficiency yields to total variation of solar efficiency between 2% to 30%, as shown in Figure 8-a. This variation is due to the change in power ratio of the solar panels, since the actual electrical power of panels varies from 0.07 to 0.35 with respect to the maxiumum electrical power of PVT system, as shown in Figure 8-b.

The geothermal loop of 300 m length can provide heat of 16.3 kW, as shown in Figure 9A, to raise the flow temperature by 20°C over the year. The inlet temperature ranges from 17°C to 27°C, while the exit temperature ranges from 37°C to 47°C. The energetic efficiency reaches between 170% and 210%. To the contrary, the

TABLE 10 Energy loads, exergy destruction, and efficiencies for each component

Component	$\dot{Q}$ [kW]	$\dot{W}$ [kW]	$\dot{S}_{gen}$ [kW/K]	$\dot{E}x_{des}$ [kW]	IR_i [%]	η [%]	ψ [%]
Building heating load	13.8	—	—	—	—	—	—
Incident solar load	0.5608	—	—	—	—	—	—
Solar collectors (M)	0.008	0.050	0.0026	0.4808	3.83%	9.47%	8.60%
Compressor (CM)	0	2.149	0.0011	0.3276	2.61%	80.00%	84.76%
Condenser (CN)	11.634	—	0.0008	0.1991	1.59%	100.00%	74.63%
Evaporator (EV)	9.485	—	0.0006	0.2044	1.63%	100.00%	70.03%
Expansion valve (EX1)	0	0	0.0003	1.8676	14.88%	100.00%	40.04%
Expansion valve (EX2)	0	0	0.0003	0.0011	0.01%	100.00%	90.60%
Expansion valve (EX3)	0	0	0.0002	0.6222	4.96%	100.00%	50.06%
Expansion valve (EX4)	0	0	0.0012	0.3549	2.83%	100.00%	88.56%
Thermal battery	9.0324	—	2.21E-02	0.0260	0.21%	90.62%	20.10%
Geothermal loop	16.7986	—	0.0581	0.0006	0.00%	99.86%	99.96%
Distributor unit	0	—	0	0	0.00%	100.00%	100.00%
Collector unit	0	—	0.0003	0.6930	5.52%	100.00%	42.20%
Transfer tank	0.9924	—	0.0131	0.7093	5.65%	96.85%	35.79%
Tank TL	8.7843	—	0.0434	0.3409	2.72%	52.22%	60.25%
Tank TH	—	6.417	0.0075	6.1848	49.27%	39.05%	3.85%
Pump (P1)	—	0.03	2.88E-05	0.0099	0.08%	70.00%	66.87%
Pump (P2)	—	0.07	7.03E-05	0.0192	0.15%	70.00%	72.63%
Pump (P3)	—	0.114	1.18E-04	0.0350	0.28%	70.00%	69.28%
Pump (P4)	—	0.12	1.15E-04	0.0366	0.29%	70.00%	69.50%
Furnace heating output	1.9179	0	0.0136	0.3934	3.13%	16.41%	79.62%
Heat exchanger HX1	0	—	0.0014	0.0145	0.12%	100.00%	83.35%
Heat exchanger HX2	0	—	0.0113	0.0331	0.26%	100.00%	83.56%
Total Exergy destruction				12.554	100.00%		

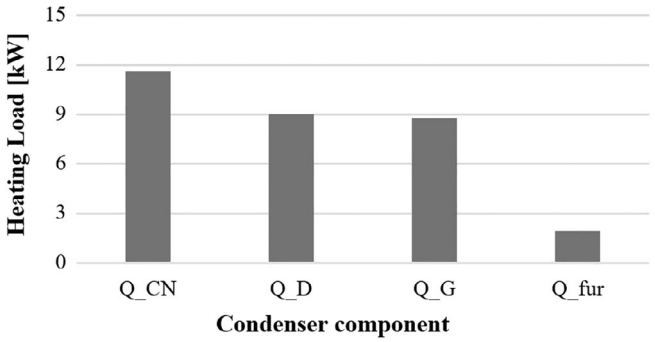

FIGURE 5 The heating load of for all condenser components

exergetic efficiency ranges between 25% and 70% because the temperature difference between the source and the standard ambient conditions.

The PCM thermal battery storage consists of two paths and PCM storage water. The first path starts from and ends to the transfer tank as state points of 2 and 5, respectively. The second path is connected to the condenser of the heat pump of state points 29 and 4. The temperature difference between the inlet and outlet flow rate of the first (T[2] and T[5]) and second path (T[4] and T[29]) are 12°C and 12°C, respectively, as shown in Figure 10A. This constant temperature difference has caused constant heat transfer for each element of thermal storage, as shown in Figure 10B.

There are three major heat components: the heat transfer from the transfer tank to the thermal storage denoted as Q_geo_PCM, which is a combination of geothermal energy, solar energy, and the thermal storage energy; the internally stored energy in the PCM storage fluid denoted by Q_PCM_internal; and the heat transfer from to the condenser of heat pump denoted by Q_PCM_HP, which equals to Q_D in Figure 5. The values of Q_geo_PCM, Q_PCM_internal, and Q_PCM_HP are determined to be 10.5, 1.2, and 9 kW, respectively, as shown in

Figure 10B. The heat loss to the soil is estimated to be between 0.2 and 0.5 kW during the year. The initial and final temperatures of stored water are 20°C and 16°C after 2 days in a month. The thermal efficiency of the thermal storage is constant of 90%, while the exergetic efficiency varies between 76% and 94% because of change in temperature, as shown in Figure 10C.

The charging fluid and discharging fluid have a constant temperature difference (12°C), as shown in Figure 11. The time for charging and discharging fluid is

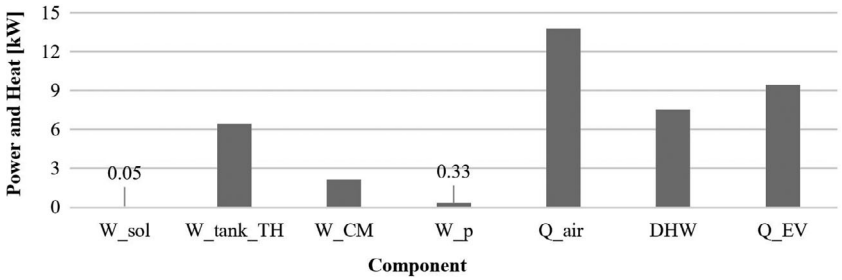

FIGURE 6 The power and heat transfer for the system components

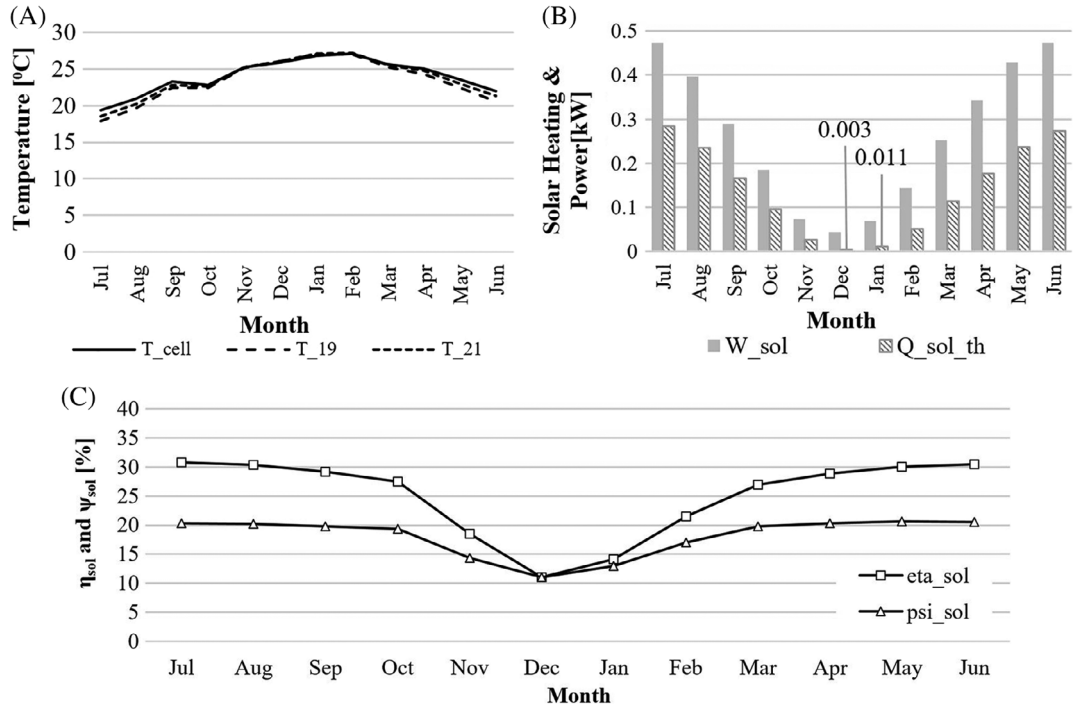

FIGURE 7 The analysis of PVT solar panel over the year. A, The inlet, exit, and cell temperature. B, The power and thermal heat. C, The energetic and exergetic efficiencies

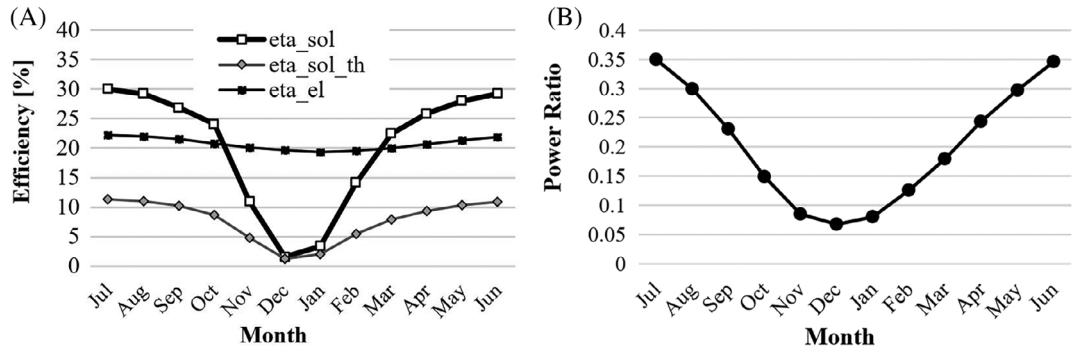

FIGURE 8 The variation of thermal, electrical and total solar efficiency and power ratio over the year. A, Thermal, electrical, and total efficiency. B, The power ratio

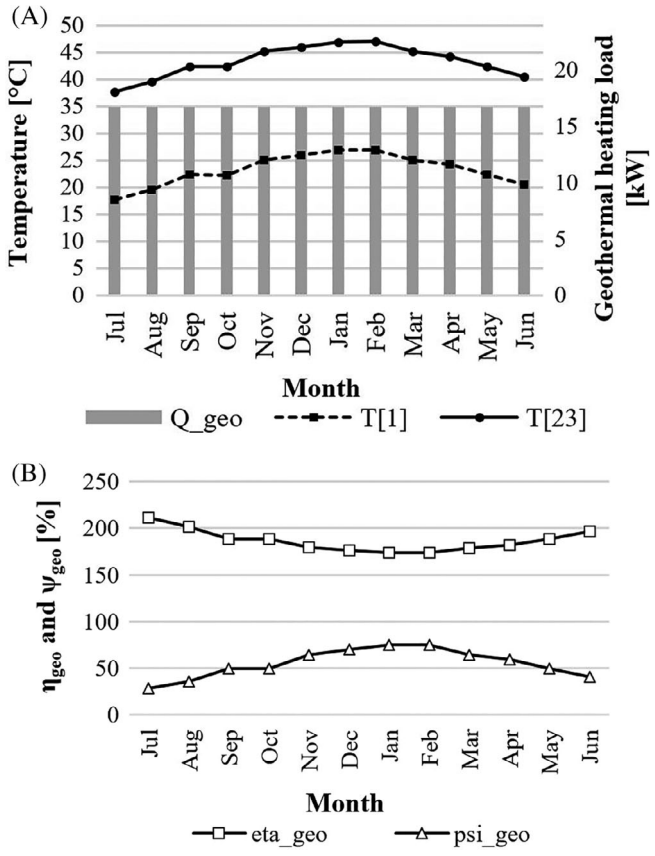

FIGURE 9 The distribution of temperature, heat load, energy efficiency, and exergy efficiency of geothermal loop over the year. A, The temperature and heat load distribution. B, The energetic and exergetic efficiencies

1 day, while the storing time is 4 days. This will give a chance for the PCM fluid to be heated to from 20°C to more than 40°C and drops again below 20°C reaching to 10°C by the end of January. The heat loss in the soil for the depth of 5 m is shown in Figure 13. The maximum heat loss is in January (0.844 kW), while the minimum heat loss occurs in July (0.0204 kW).

The temperature distribution of the PCM storage fluid is displayed in Figure 12 over the year. The process starts the operations from the beginning of July at the initial temperature of 20°C. As shown in Figure 12, the PCM temperature at the storing period increases to 42°C in July to 52°C in October then drops to about 30°C in April and May. In addition, the PCM temperature at the end of the discharging period increases from 22°C in July to 31°C in October and drops to 7°C in April and May. The main reason for this increase and decrease in the PCM fluid temperature is the change of heat loss in the soil every month, as shown in Figure 13.

The inlet flow rate to the transfer tank stated as point 24 combines all the flows from the geothermal loop, thermal battery, and solar panels with a temperature of 15.5°C in July to 24.5°C in February, as shown in Figure 14. The transfer tank is used to store the fluid and retransfer it to a geothermal loop, thermal battery storage, and solar panels with almost the same temperature since the heat loss of the transfer tank are negligible.

The heating load of the integrated system is the summation of heat from the thermal battery and the condenser, which are constant over the year. However, the furnace is adding heat to cover the shortage of heating load based on the heating load of the building, as shown in Figure 15A, which occurs in January (1.84 kW) and February (0.29 kW). Also, the power consumption of the compressor and pumps are constant during the year with values of 2.2 kW and 0.34 kW, respectively. However, the supplied power by the solar panels is varied and has a maximum value of 0.5 kW, as shown in Figure 15B.

As shown in Table 11, the overall energetic and exergetic COP of the integrated system are 52.0% and 3.34% in the heating season and 42.6% and 4.47% in the cooling season, respectively. The value of energetic COP for heating season includes the furnace heating load (1.84 kW) to provide the total heating load of the building. The total output energy for cooling season is less than that of heating season because the building in Oshawa has a cooling load less than heating load. The exergetic COP is very low because the total input exergy rate is high due to the high input power from the compressor, pumps, and electric heater of tank TH, which are more than double the thermal exergy rate.

To evaluate the proposed system, a performance comparison is established between the proposed system and traditional systems such as furnace only and furnace with heat pump, especially in the heating season, as shown in Table 12. The integrated system uses a furnace for heating by 1.837 kW. While using the furnace only for heating the building and providing the hot water, the furnace heating load will be 28.45 kW. In the case of using furnace heat for only hot water, the furnace heating load will be 14.64 kW. That means the proposed integrated system saves about 93% of furnace heating load and the used propane fuel. In another way, the proposed system will eliminate the home's propane usage to be eco-friendly system.

Using the heat pump only for heating the building needs a large capacity heat pump which translates into a large condenser load (13.8 kW) and a large compressor load (3.75 kW), while using the renewable sources have increased the heating load of the condenser but decreased the compressor power to 2.149 kW. This saves the power consumption of heat pump by about 43%. Therefore, the COP for the heat pump is increased about 2-fold from 358% to 642.2% for the heating season and 268% to 441.4% for the cooling season, as shown in Table 12.

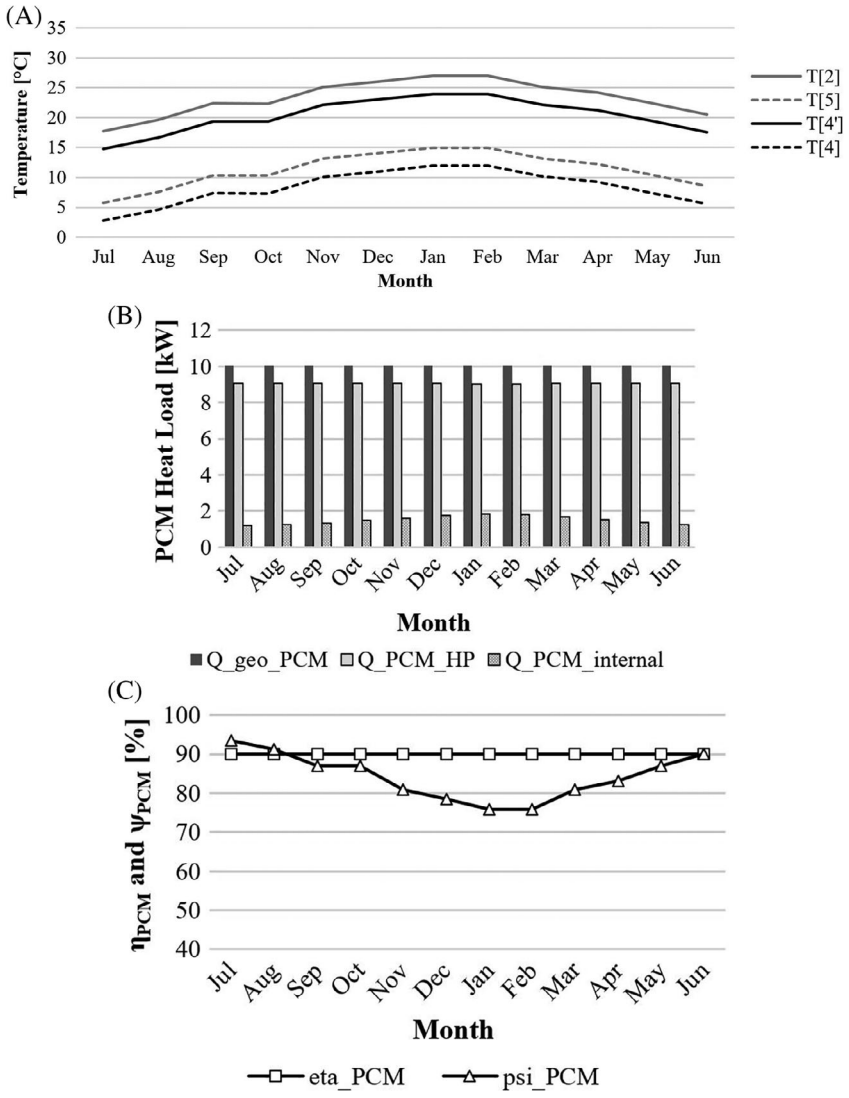

FIGURE 10 The PCM thermal battery storage analysis over the year. A, Temperature distribution of inlet and exit flow of the PCM thermal battery storage. B, The heat transfer distribution. C, The energetic and exergetic efficiency

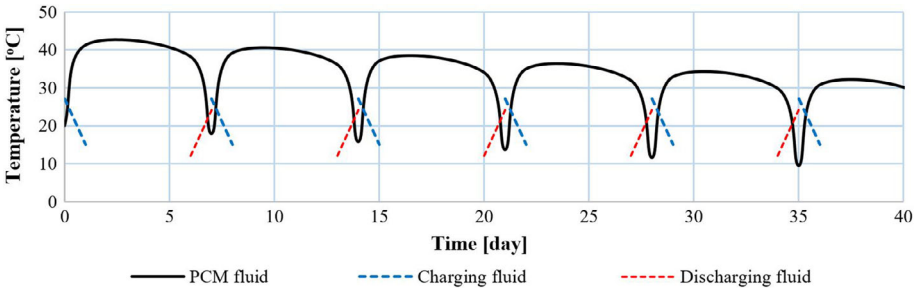

FIGURE 11 The temperature distribution of charging, discharging, and PCM storage over the days in January

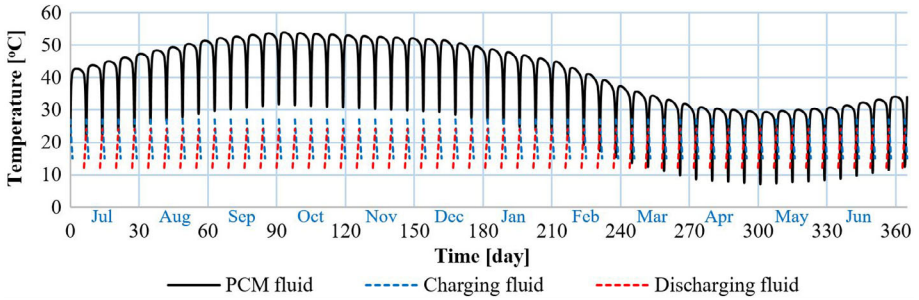

FIGURE 12 The temperature distribution of charging, discharging, and PCM storage over the year starting from July

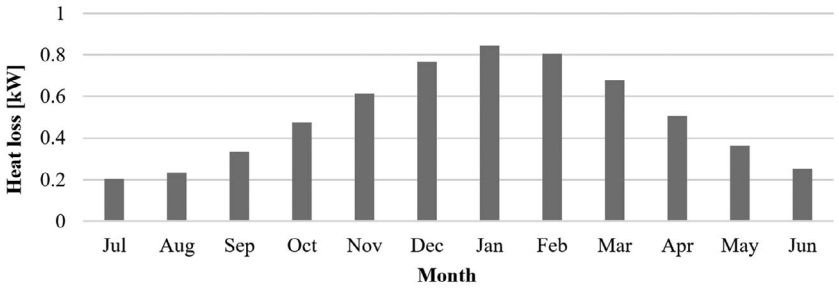

FIGURE 13 The soil heat loss from 5 m under the ground surface over the year

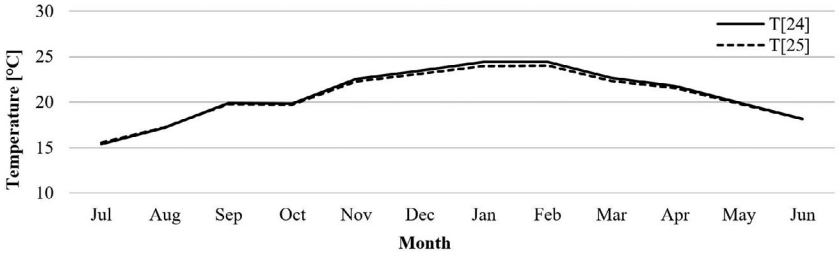

FIGURE 14 The temperature of inlet exit flow of transfer tank (A)

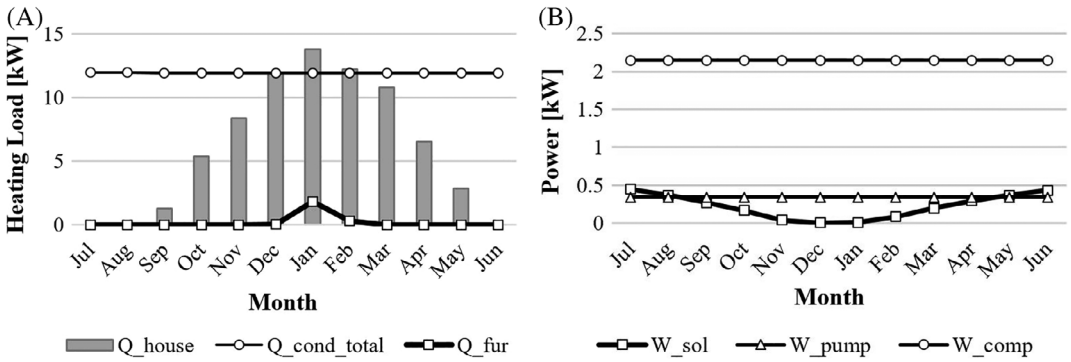

FIGURE 15 The distribution of total heat and power of the hybrid system over the year. A, The heating load of the building, condenser coils, and the furnace. B, The power of solar panels, pumps, and compressor

TABLE 11 Overall performance of the integrated system

Parameters	Heating season (January)	Cooling season (July)
Total input energy [kW]	41.08	41.01
Total output energy [kW]	21.35	17.47
COP_{en}	52.0 %	42.6%
COP_{ex}	3.34%	4.47%

TABLE 12 A comparison between the integrated system and other systems

	Integrated system	Furnace only	Heat pump and furnace
Furnace heating load [kW]	1.84	28.45	14.64 (for DHW)
Propane mass flow rate [kg/min]	0.014	0.208	0.106 (for DHW)
Condenser heating load [kW]	13.8	0	13.8
Evaporator heat rejection [kW]	9.49	0	10.05
Compressor power [kW]	2.149	0	3.75
Heat pump COP for heating	642.2%	0	368.0%
Heat pump COP for cooling	441.4%	0	268%

5 | CONCLUSION

Most Canadian buildings use furnaces for heating and providing domestic hot water. The proposed system uses renewable sources such as solar energy, geothermal energy, and thermal storage energy to eliminate the propane used for heating. A case study of a residential building with three floors in Oshawa was selected using the proposed system. The heating load of the building is 13.8 kW, and the heating load for the domestic hot water is 7.5 kW. The building is equipped with five PVT solar panels, a 300 m length of geothermal loop, and 9463.53 kg of water PCM thermal battery storage. The following conclusions can be drawn:

- The solar panels increase the water flow temperature from 0.05°C to 1°C and provide the maximum power of 0.5 kW and the maximum thermal load of 0.3 kW.
- The geothermal loop can increase the temperature of the water flow by 20°C with a heating load of 16.3 kW.
- The PCM thermal battery storage provides a heating load of 9 kW to the condenser to increase the water temperature by 10°C.
- The total heating load of the condenser without the furnace load reaches 11.9 kW, and the furnace heating load is 1.85 kW to provide the required heating load of the building.
- The overall energetic COP is obtained to be 52% with the furnace load and 54.58% without the furnace heating load. The exergetic COP is 3.34% for the heating season.
- The energetic and exergetic COP are obtained to be 42.9% and 4.447% for the cooling season.
- The integrated system eliminates the propane usage by 93% over the year. The propane mass flow rate is 0.014 kg/min in the winter season.
- The COP of the heat pump is doubled to 642.2% compared to the case of using heat pump only for heating the building.
- The usage of renewable systems has saved the power consumption of the heat pump by 43%.

ACKNOWLEDGMENT

This research is supported by the Natural Sciences and Engineering Research Council of Canada (NSERC).

ORCID

Shaimaa Seyam https://orcid.org/0000-0002-9780-697X
Ibrahim Dincer https://orcid.org/0000-0002-7092-2102

REFERENCES

1. Natural Resources Canada. *Heating Equipment for Residential Use*; 2018. https://www.nrcan.gc.ca/energy/products/categories/heating/13740. Accessed January 2, 2019.
2. Kampa M, Castanas E. Human health effects of air pollution. *Environ Pollut*. 2008;151:362-367. https://doi.org/10.1016/j.envpol.2007.06.012
3. Seyam S, Al-hamed KHM, Qureshy AMMI, Dincer I. Multi-objective Optimization of Hydrogen Production in Hybrid Renewable Energy Systems. *IEEE Congr. Evol. Comput.* Wellington, New Zealand, 2019, p. 850-857.
4. Shabgard H, Song L, Zhu W. Heat transfer and exergy analysis of a novel solar-powered integrated heating, cooling, and hot water system with latent heat thermal energy storage. *Energ Conver Manage*. 2018;175:121-131. https://doi.org/10.1016/j.enconman.2018.08.105
5. Islam S, Dincer I, Yilbas BS. Development, analysis and assessment of solar energy-based multigeneration system with thermoelectric generator. *Energ Conver Manage*. 2018;156:746-756. https://doi.org/10.1016/j.enconman.2017.09.039
6. Joshi AS, Dincer I, Reddy BV. Performance analysis of photovoltaic systems: a review. *Renew Sustain Energy Rev*. 2009;13:1884-1897. https://doi.org/10.1016/j.rser.2009.01.009
7. Kalogirou SA, Karellas S, Braimakis K, Stanciu C, Badescu V. Exergy analysis of solar thermal collectors and processes. *Prog Energy Combust Sci*. 2016;56:106-137. https://doi.org/10.1016/j.pecs.2016.05.002
8. Krismadinata RNA, Ping HW, Selvaraj J. Photovoltaic module modeling using Simulink/Matlab. *Procedia Environ Sci*. 2013;17:537-546. https://doi.org/10.1016/j.proenv.2013.02.069
9. Ozgener O. Use of solar assisted geothermal heat pump and small wind turbine systems for heating agricultural and residential buildings. *Energy*. 2009;35:262-268. https://doi.org/10.1016/j.energy.2009.09.018
10. Chang S, Madani H, Palm B. Heating solutions for residential buildings in China: current status and future outlook. *Energ Conver Manage*. 2018;177:493-510. https://doi.org/10.1016/j.enconman.2018.10.005
11. Seyam S. *Types of HVAC Systems. HVAC Syst.* London, UK: IntechOpen; 2018, p. 49-66. https://doi.org/10.5772/intechopen.78942
12. Bayer P, Saner D, Bolay S, Rybach L, Blum P. Greenhouse gas emission savings of ground source heat pump systems in Europe: a review. *Renew Sustain Energy Rev*. 2012;16:1256-1267. https://doi.org/10.1016/J.RSER.2011.09.027
13. Banks D. *An Introduction to Thermogeology: Ground Source Heating and Cooling*. 2nd Edition. Oxford, UK: Wiley-Blackwell; 2012. https://doi.org/10.1002/9781118447512.
14. Watzlaf GR, Ackman TE, Williams WA. Underground mine water for heating and cooling using geothermal heat pump systems. *Mine Water Environ*. 2006;25:1-14.
15. Li H, Sun L. Feasibility analysis of solar assisted ground-coupled heat pump indirect heating systems. *Procedia Eng*. 2017;205:826-833. https://doi.org/10.1016/j.proeng.2017.10.018
16. Liang CH, Zhang XS, Li XW, Zhu X. Study on the performance of a solar assisted air source heat pump system for building heating. *Energy Build*. 2011;43:2188-2196. https://doi.org/10.1016/j.enbuild.2011.04.028
17. Latorre-Biel JI, Jiménez E, García JL, Martínez E, Jiménez E, Blanco J. Replacement of electric resistive space heating by an

air-source heat pump in a residential application. Environmental amortization. *Build Environ*. 2018;141:193-205. https://doi.org/10.1016/j.buildenv.2018.05.060

18. Michopoulos A, Martinopoulos G, Papakostas K, Kyriakis N. Energy consumption of a residential building: comparison of conventional and RES-based systems. *Int J Sustain Energy*. 2009;28:19-27. https://doi.org/10.1080/14786450802452373
19. Zhang Y, Qi DW, Wang WJ, Lv ZY. Study of solar energy floor heating system in cold climate zone. *Appl Mech Mater*. 2012; 193–194:146-151. https://doi.org/10.4028/www.scientific.net/AMM.193-194.146
20. Tahersima M, Tikalsky P, Revankar R. An experimental study on using a mass radiant floor with geothermal system as thermal battery of the building. *Build Environ*. 2018;133:8-18. https://doi.org/10.1016/j.buildenv.2018.02.010
21. O'Shaughnessy E, Cutler D, Ardani K, Margolis R. Solar plus: optimization of distributed solar PV through battery storage and dispatchable load in residential buildings. *Appl Energy*. 2018;213:11-21. https://doi.org/10.1016/j.apenergy.2017.12.118
22. Georgakarakos AD, Mayfield M, Hathway EA. Battery storage systems in smart grid optimised buildings. *Energy Procedia*. 2018;151:23-30. https://doi.org/10.1016/j.egypro.2018.09.022
23. Beausoleil-Morrison I, Kemery B, Wills AD, Meister C. Design and simulated performance of a solar-thermal system employing seasonal storage for providing the majority of space heating and domestic hot water heating needs to a single-family house in a cold climate. *Sol Energy*. 2019;191:57-69. https://doi.org/10.1016/j.solener.2019.08.034
24. Wills A, Cruickshank CA, Beausoleil-Morrison I. Application of the ESP-r/TRNSYS co-simulator to study solar heating with a single-house scale seasonal storage. *Energy Procedia*. 2012;30:715-722. https://doi.org/10.1016/j.egypro.2012.11.081
25. Antoniadis CN, Martinopoulos G. Optimization of a building integrated solar thermal system with seasonal storage using TRNSYS. *Renew Energy*. 2019;137:56-66. https://doi.org/10.1016/j.renene.2018.03.074
26. F-Chart Software: Engineering Software. *EES: Engineering Equation Solver*. http://fchartsoftware.com/ees/. Accessed September 25, 2019.
27. Klein SA. Development and integration of an equation-solving program for engineering thermodynamics courses. *Comput Appl Eng Educ*. 1993;1:265-275. https://doi.org/10.1002/cae.6180010310
28. Dincer I, Rosen MA. *Exergy: Energy, Environment And Sustainable Development*. 2nd ed. Oxford, UK: Elsevier; 2013.
29. Yazdanpanahi J, Sarhaddi F, Mahdavi Adeli M. Experimental investigation of exergy efficiency of a solar photovoltaic thermal (PVT) water collector based on exergy losses. *Sol Energy*. 2015;118:197-208. https://doi.org/10.1016/j.solener.2015.04.038
30. Herrando M, Markides CN, Hellgardt K. A UK-based assessment of hybrid PV and solar-thermal systems for domestic heating and power: system performance. *Appl Energy*. 2014;122:288-309. https://doi.org/10.1016/j.apenergy.2014.01.061
31. Tiwari A, Dubey S, Sandhu GS, Sodha MS, Anwar SI. Exergy analysis of integrated photovoltaic thermal solar water heater under constant flow rate and constant collection temperature modes. *Appl Energy*. 2009;86:2592-2597. https://doi.org/10.1016/j.apenergy.2009.04.004
32. Tiwari A, Sodha MS. Performance evaluation of solar PV/T system: an experimental validation. *Sol Energy*. 2006;80:751-759. https://doi.org/10.1016/j.solener.2005.07.006
33. Carrier Building Solutions. *Hourly Analysis Program HVAC System Design Software*. https://www.carrier.com/commercial/en/us/software/hvac-system-design/hourly-analysis-program/. Accessed September 25, 2019.
34. Natural Resources Canada. *RETScreen*. https://www.nrcan.gc.ca/energy/retscreen/7465. Accessed September 25, 2019.
35. TESZEUS® Photovoltaic-Thermal Hybrid Solar Collector.
36. Gas/Oil Boilers – TES Group Limited. *Solar Water Heater, PV-T Hybrid Collectors*. http://www.tessolarwater.com/. Accessed September 25, 2019.
37. Dinçer I, Kanoglu M. *Refrigeration Systems and Applications*. 2nd ed. New York: Wiley; 2010.
38. Chow TT, He W, Ji J. Hybrid photovoltaic-thermosyphon water heating system for residential application. *Sol Energy*. 2006;80:298-306. https://doi.org/10.1016/j.solener.2005.02.003
39. Lee B, Liu JZ, Sun B, Shen CY, Dai GC. Thermally conductive and electrically insulating EVA composite encapsulant for solar photovoltaic (PV) cell. *Express Polym Lett*. 2008;2:357-363. https://doi.org/10.3144/expresspolymlett.2008.42
40. Naterer GF. *Advanced Heat Transfer*. 2nd ed. Boca Raton, FL: Taylor & Francis, CRC Press; 2018. https://doi.org/1037//0033-2909.I26.1.78

How to cite this article: Seyam S, Dincer I, Agelin-Chaab M. Thermodynamic analysis of a hybrid energy system using geothermal and solar energy sources with thermal storage in a residential building. *Energy Storage*. 2019;e103. https://doi.org/10.1002/est2.103